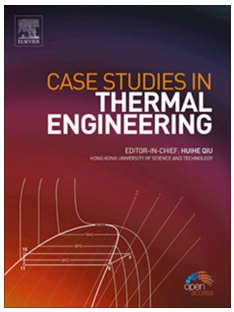

Numerical study of free convection in a thin layer between coaxial horizontal cylinders

Alexander Fedotov, Yana Tsitavets, Andrey Elyshev

PII: S2214-157X(22)00843-7

DOI: https://doi.org/10.1016/j.csite.2022.102606

Reference: CSITE 102606

To appear in: *Case Studies in Thermal Engineering*

Received Date: 21 September 2022

Revised Date: 12 November 2022

Accepted Date: 26 November 2022

Please cite this article as: A. Fedotov, Y. Tsitavets, A. Elyshev, Numerical study of free convection in a thin layer between coaxial horizontal cylinders, *Case Studies in Thermal Engineering* (2022), doi: https://doi.org/10.1016/j.csite.2022.102606.

Numerical study of free convection in a thin layer between coaxial horizontal cylinders

Alexander Fedotov[a,b,*] , Yana Tsitavets[a,b], Andrey Elyshev[a]

[a]*Nature-inspired engineering center, University of Tyumen, Volodarskogo Str. 6, Tyumen, 625003, Russia*

[b]*Physics Faculty, Belarusian State University, Nezalezhnasci av., 2, Minsk, 220030, Belarus.*

Abstract

We consider free convection in 2D and 3D horizontal cylindrical layers with the inner hot and outer cold boundary at Ra (Rayleigh number) in range ($4\cdot10^3 \div 4\cdot10^5$) and the ratio $\delta \approx 1{:}20$ of the layer width to inner radius. Prandtl number was 0,71, fluid properties were taken for air at 293 K.

It was shown that the flow in a 2D cylindrical layer can be divided into three regions. Stable symmetric convective rolls are formed in the layer's upper part; regions with the transient flow appear at the lateral sides; transitional regions between the upper and the lateral regions have convective rolls of an unusual asymmetric shape.

The flow in a 3D cylindrical layer in the upper part is organized into a spatially stable convective roll pattern. With increase of the Rayleigh number (Ra), roll pattern becomes suppressed by a transient plume pattern.

The global Nu (the Nusselt number) is proportional to $0{,}0019\cdot Ra^{0{,}567}$ for the 2D case and to $0{,}22\cdot Ra^{0{,}192}$ for the 3D case. The 2D problem provides a reasonable estimation of the Nusselt number for Rayleigh number up to $4\cdot10^4$ and overestimates Nu for higher Rayleigh number, which agrees with Lyapunov exponent values.

Keywords: *convection, Rayleigh-Bénard, Nusselt, Lyapunov, coaxial cylinders*

Nomenclature	
$\vec{v}$	flow velocity, m/s
P	pressure, Pa
T	temperature, K
ρ	density, kg/m^3
t	time, s
β	volumetric temperature expansion coefficient, K^{-1}
χ	thermal diffusivity, m^2/s
ν	kinematic viscosity, m^2/s
g	free fall acceleration, m/s^2
η	Kolmogorov scale, m
η_B	Batchelor scale, m
Λ	Lyapunov exponent, s^{-1}
φ	angular coordinate, º
R	internal radius of cylinder, m
T_{cold}	temperature of cold boundary, K
T_{hot}	temperature of hot boundary, K
L	distance between coaxial cylinders, m
$\vec{q}_i$	coordinates of particle, m
$\Delta_{i,s}$	distance between *i*-pair of particles at time *s*, m

* *Corresponding author.

Email addresses: fedotov.alehandro@gmail.com (Alexander Fedotov), yoscrimmer@gmail.com (Yana Tsitavets)

1. Introduction

Convective flow is one of the major heat transfer mechanism. It influences the formation of clouds [1] and volcanic basalt columns [2], thawing of ice [3], solar granulation [4], etc. Convective instability defines heat transfer in many functional devices: heat exchangers, nanostructure deposition setups [5], cooling systems [6], nuclear reactors [7–9] and particle accelerators [10–12]. Thus, understanding and controlling convective flow remains an important topic of physics and thermal engineering research.

The thin cylindrical layer is a remarkable physical system. On the one hand, it can be divided into almost plane-parallel fragments; on the other hand, these fragments are interconnected, and each of them is inclined differently with respect to gravity from neighboring fragments. The consideration of such a system will make it possible to bind the concepts of traditional Rayleigh-Bénard convection and convection in a more complex curved geometry. Convection in a thin layer between coaxial horizontal cylinders is important for numerous engineering applications, including solar concentrators [13], thermal screens of particle accelerator setups [12,14,15], power cables [16], and others.

Convection in a horizontal cylindrical layer has drawn prodigious attention in recent years. A. Passerini and coauthors proved the stable flows existence for such a system by studying the Oberbeck–Boussinesq equations [17]. Y. Wang and others showed that the fluid circulation intensifies the heat transfer in a most significant way in the narrow regions above and below the cylinder [18]. H. Majdi and colleagues proved that the radius ratio between inner and outer cylinders has a fundamental impact on the flow character [19]. However, the above-mentioned research considers a thick cylindrical layer with a width of the same order of magnitude as the cylinders' radius. J.-S. Yoo considered the two-dimensional thin layer with a ratio of width to the inner radius $\delta = 1{:}12$. It was found out that thermal instability creates a series of counter-rotating cells, which differs as from the flow in a thick cylindrical layer and Rayleigh-Bénard cells [16,20].

Recent studies showed that Nu number increases and buoyancy-driven convection intensifies with Ra in thin crescent cavities [21]. In case of magnetohydrodynamic mixed convection due to a rotation of a cylinder in a trapezoidal enclosure filled with nanofluid, the average Nusselt number may be increased by raising the Hartmann number, thermal conductivity and the cylinder radius [22]. The convection phenomena in such a system is strongly affected by the Reynolds and Richardson numbers [23]. A.K. Hussein et. al. have established that the radius and alignment of internal cylinder can significantly change heat transfer properties in a cavity [24,25]. It was shown that conduction mechanism dominates between two coaxial inclined cylinders at low Ra, and that the highest Nu number is achieved at 90° inclination angle [26]. Mallikarjuna and coauthors showed that thermophoretic porous flow past horizontal conical body can be described by ordinary differential equations, where velocity at surface of body can be increased by tuning the amount thermal radiation of Darcy and Forchheimer parameters [27]. Elkhazen and coauthors explored electroconvection in an elliptical annulus and found that unipolar charge injection from the internal electrode significantly changes the topology of the flow with a formation of multicellular convective pattern [28].

Thus, free convection in a thin cylindrical layer is of interest both from a fundamental and an applied point of view. Because thin layers have received relatively low attention, we decided to focus our research on them in this study. The thin layer's geometric characteristics corresponds to the interval between the thermal screen and the heat source in Time-Projection Chamber of Multi-Purpose Detector setup of NICA (Nuclotron based Ion Collider fAcility) [11,12]. Deeper understanding of this flow type will benefit to thermal engineering via optimization of heat spatial distribution in thermal systems.

The study of convection in a thin curved layer is computationally challenging. The meshing

of curved smooth domain boundaries leads to a significant increase in the cells number in comparison with flat boundaries. However, modern codes for finite-element analysis support computational meshes with different shapes, aspect ratios, and orientations of cells [29,30]. This makes the meshes optimization possible and opens new perspectives for computational studies of flows in complex domains. We chose the COMSOL Multiphysics code since it provides a state-of-the-art implementation of the finite element method (FEM) and an appropriate mesh generator.

In this work, we study free convection in a horizontal cylindrical layer with the inner hot and the outer cold boundary. We explore the dynamics of convective flow including the spatial shape of convective cells, type of convective pattern, mixing regime and Nusselt number. Both the two-dimensional and three-dimensional cases are compared in order to check if there is noticeable difference in heat transfer properties. The ratio of layer width to the inner radius is $\delta = 1{:}20$, and the Rayleigh number is in range $(4\cdot10^3 \div 4\cdot10^5)$.

2. Simulation details

Let us consider a two-dimensional (2D) and three-dimensional (3D) problem of convection in a thin cylindrical layer. The initial-boundary value problem was set up for the Navier-Stokes equations for an incompressible fluid in the Boussinesq approximation [31] :

$$\begin{cases} \dfrac{\partial \vec{v}}{\partial t} + (\vec{v}\nabla)\vec{v} = -\dfrac{1}{\rho_0}\nabla P + \nu\Delta\vec{v} + g\beta T\vec{e}_z, \\ \nabla\cdot\vec{v} = 0, \\ \dfrac{\partial T}{\partial t} + \vec{v}\cdot\nabla T = \chi\Delta T, \\ \rho(T) = \rho_0(1-\beta(T-T_0)) \end{cases} \tag{1}$$

where $\vec{v}$ is the flow velocity, P is the pressure, T is the temperature, ρ is the density, t is the time, g is the gravitational constant, β is the coefficient of thermal expansion, χ is the thermal diffusivity, ν is the viscosity, ρ_0 is the fluid density at the reference temperature T_0.

The scheme of the computational domain is given in Figure 1a,b. We considered solid nonslip walls with T_{hot} temperature at the inner boundary Γ_{in} and T_{cold} temperature at the outer boundary Γ_{out}. Boundary conditions for the 2D problem are given in (2), and for the 3D problem in (3):

$$\vec{v} = 0,\ x,y \in \Gamma_{in},\Gamma_{out}; \qquad T = T_{hot},\ x,y \in \Gamma_{in}; \qquad T = T_{cold},\ x,y \in \Gamma_{out} \tag{2}$$

$$\vec{v} = 0,\ x,y \in \Gamma_{in},\Gamma_{out}; \quad T = T_{hot},\ x,y \in \Gamma_{in}; \quad T = T_{cold},\ x,y \in \Gamma_{out}; \quad \vec{v}\big|_{z=0} = \vec{v}\big|_{z=z_{\max}},\ T\big|_{z=0} = T\big|_{z=z_{\max}},\ x,y \in \Gamma_{p1},\Gamma_{p2} \tag{3}$$

The Rayleigh number governs the intensity of free convection and is given by the following expression [32]:

$$\mathrm{Ra} = \frac{g\beta(T_{hot} - T_{cold})L^3}{\nu\chi}, \tag{4}$$

where L is the characteristic height,. The Rayleigh number was set up by varying the temperature T_{hot} at the inner boundary. We considered the Prandtl number Pr = 0,71 as well as material properties for air.

Equations (1) with conditions (2),(3) were solved in Cartesian coordinates by a finite-element

method implemented in the COMSOL Multiphysics [33]. Velocity, pressure, and temperature fields were approximated by second-order Lagrange polynomials. Polynomial coefficients were found from the corresponding systems of linear equations, which were solved by the LU-decomposition method (PARDISO library [34–36]). Time integration was performed using the implicit time-dependent solver based on second-order backward differentiation formula [37–39]. Time step did not exceed $1 \cdot 10^{-3}$ s. COMSOL testing and verification for known free convection problems is described in details in Appendix A.

Parts of computational meshes are shown in Figures 1c, d. The final meshes included about 10^5 elements for the 2D problem and about 10^7 elements for the 3D one. In order to accurately capture the features of the flow, mesh resolution has to be at least of the same order of magnitude as the Kolmogorov scale η and Batchelor scale η_B [40–42]:

$$\eta = \frac{L\,\mathrm{Pr}^{1/2}}{\left(\mathrm{Ra}\cdot(\mathrm{Nu}-1)\right)^{1/4}}; \qquad \eta_B = \eta\,\mathrm{Pr}^{-1/2} \tag{5}$$

As further computations have shown (chapter 4), Nu number does not exceed 3.5, which leads to η in range (0,0018 ÷ 0,0126) m and η_B in range (0,0021 ÷ 0,0150) m for $\mathrm{Ra} = 4 \cdot 10^5$. In this study mesh elements had linear sizes about $\Delta_{2D} \approx 0{,}0019$ m in the 2D case and $\Delta_{3D} \approx 0{,}0023$ m which is enough to study the convective flow under given conditions.

The Lyapunov exponent Λ is a useful indicator for quantifying the intermixing in the flow [43]. The negative Lyapunov exponent means that two points with close initial positions tend to approach each other over time, while the positive one indicates that the points tend to disperse [44].

In order to compute Λ, we traced fluid volumes in the flow using massless Lagrange particles as markers. The velocity of each particle matched the flow velocity [45]:

$$\frac{d\vec{q}_i}{dt} = \vec{v}, \tag{6}$$

where $\vec{q}_i$ are the coordinates of marker particle and $\vec{v}$ is the velocity of the fluid at coordinates $\vec{q}_i$, determined from Eqs. (1). Eqs. (6) were time-integrated with the Dormand-Prince method [46].

First, a number of randomly distributed particles were introduced to the quasistationary flow. Second, the distances $\Delta_{j,s}$ between pairs of closely located particles were calculated at time *s*. Finally, the distances for the same pairs were updated and new distances $\Delta_{j,s+1}$ were found at the next time step (*s*+1). The averaged Lyapunov exponent Λ was computed from the following expression [47]:

$$\Lambda = \frac{1}{t_{avg}} \cdot \frac{1}{N} \sum_{j=1}^{N} \ln \left| \frac{\Delta_{j,s+1}}{\Delta_{j,s}} \right|, \tag{7}$$

where *N* is the number of particle pairs in the considered volume, t_{avg} = 0,05 s is the time interval between *s* and (*s*+1) time moments. About 10^5 particles were used in each simulation.

The angular distribution Λ(φ) was computed by averaging local exponents with a 5° step. The angular coordinate φ was counted clockwise from the vertical passing through the center of the cylindrical layer (Figure 1a).

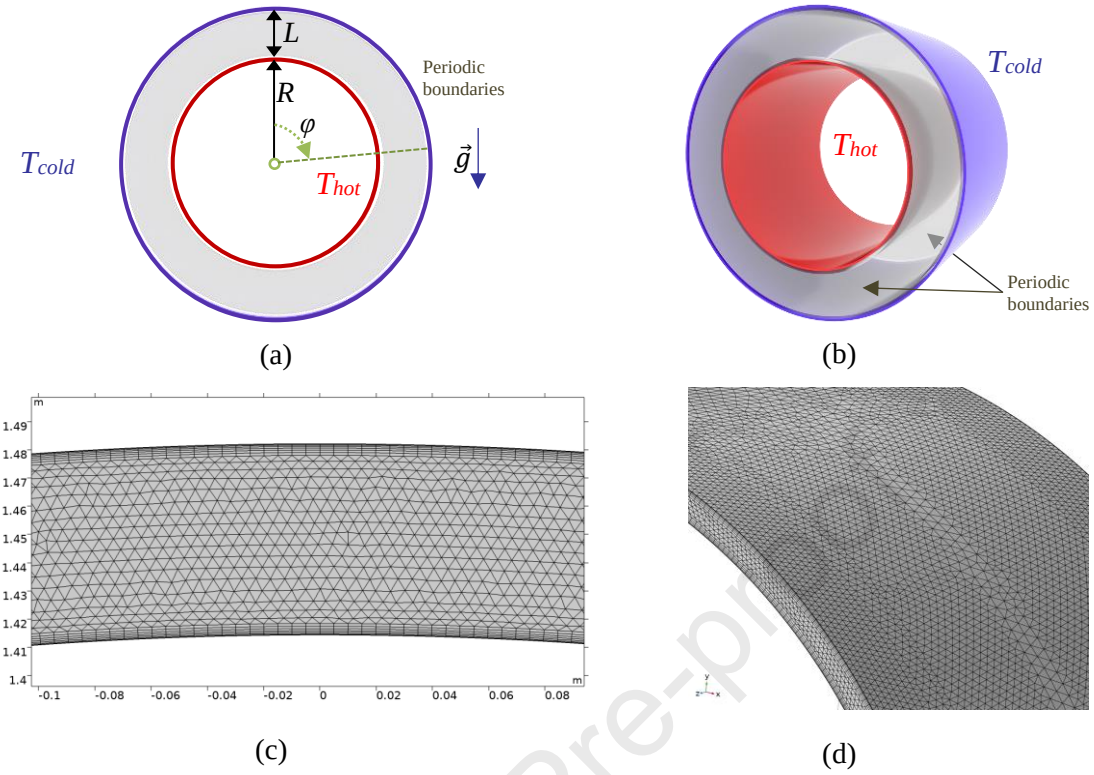

Figure 1. Computational domain scheme for the 2D (a) and 3D (b) problem, and fragments of computational meshes for the 2D (c) and 3D (d) problem.

3. Velocity and temperature distributions

We studied the temperature and velocity spatial distributions for the 2D and 3D problems. The temperature and velocity for the 2D cylindrical layer are given in Figure 2. As can be seen, there are three main regions where the flow's nature differs. The first (upper) region is located at the top of the cylindrical layer in the range of $\varphi \approx (-15° \div 15°)$. The second (transitional) region is located at $\varphi \approx \pm (15° \div 50°)$. The third (lateral) region is on the sides of the cylindrical layer at $\varphi \approx \pm (50° \div 170°)$. No convection develops in the range of $\varphi \approx (-170° \div 170°)$ because of the hot boundary located above the cold one.

The velocity and temperature in the upper region are shown in Figure 2a,b. The velocity at $Ra = 4 \cdot 10^3$ is in $(10^{-3} \div 10^{-2})$ m/s range. The temperature distribution is strongly affected by heat conduction, which leads to the smooth rolls formation (Figure 2b). At higher Rayleigh numbers, the velocity increases up to 10^{-1} m/s and the rolls have a plume shape due to the growing contribution of the convective heat transfer mechanism. This flow is similar to the classical Rayleigh-Bénard convection, except that convective rolls expand slightly with Ra (Figure 2a,b).

Starting with $Ra = 4 \cdot 10^4$, rolls appear in the transitional region (Figure 2c,d). Rolls there have an asymmetrical shape because the lower vortex in a cell is elongated. This further elongation of the lower vortex with Ra leads to the spatial expansion of the rolls as in the case of the upper region.

As in the transitional region, the flow in the lateral region arises when Ra is larger than $4 \cdot 10^3$ (Figure 2f,g). The flow is transient and does not lead to the formation of stable rolls.

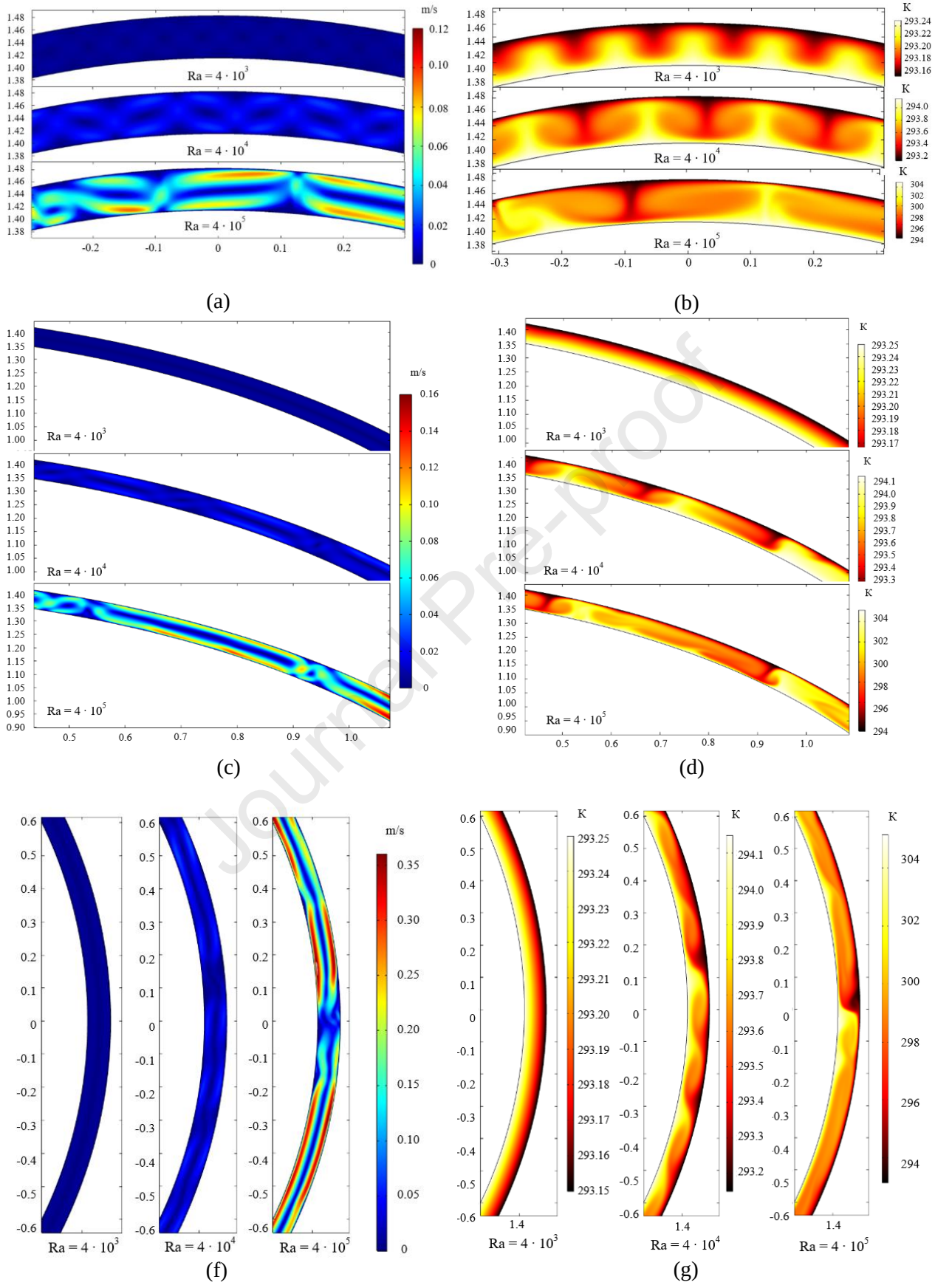

Figure 2. Velocity and temperature fields for 2D problem: velocity spatial distribution for the upper (a), transitional (c) and lateral (f) regions and temperature spatial distribution for the upper (b), transitional (d) and lateral (g) regions for different Ra

Velocity and temperature distributions for the 3D case are given in Figure 3 at the half-width of the cylindrical layer. The 3D free convection is characterized by periodic spatial pattern of

temperature distribution which is called a convective texture [48–51].

At Ra = $4 \cdot 10^3$, the flow arises only in the upper region and forms a stationary roll pattern (Figure 3a,b). This type of convective pattern is similar to Turing morphogenesis patterns [52]. It has been described by several researchers for Rayleigh-Bénard convection [48–51].

At Ra = $4 \cdot 10^4$, another type of pattern is observed in the lateral and transitional regions (Figure 3c,d). The flow in these regions consists of coherently moving plumes. Such a pattern visually resembles a combination of Rayleigh-Taylor and Rayleigh-Bénard instabilities [53,54]. With the increase of Ra to $4 \cdot 10^5$, the plume pattern changes to a chaotical flow without an obvious spatial ordering.

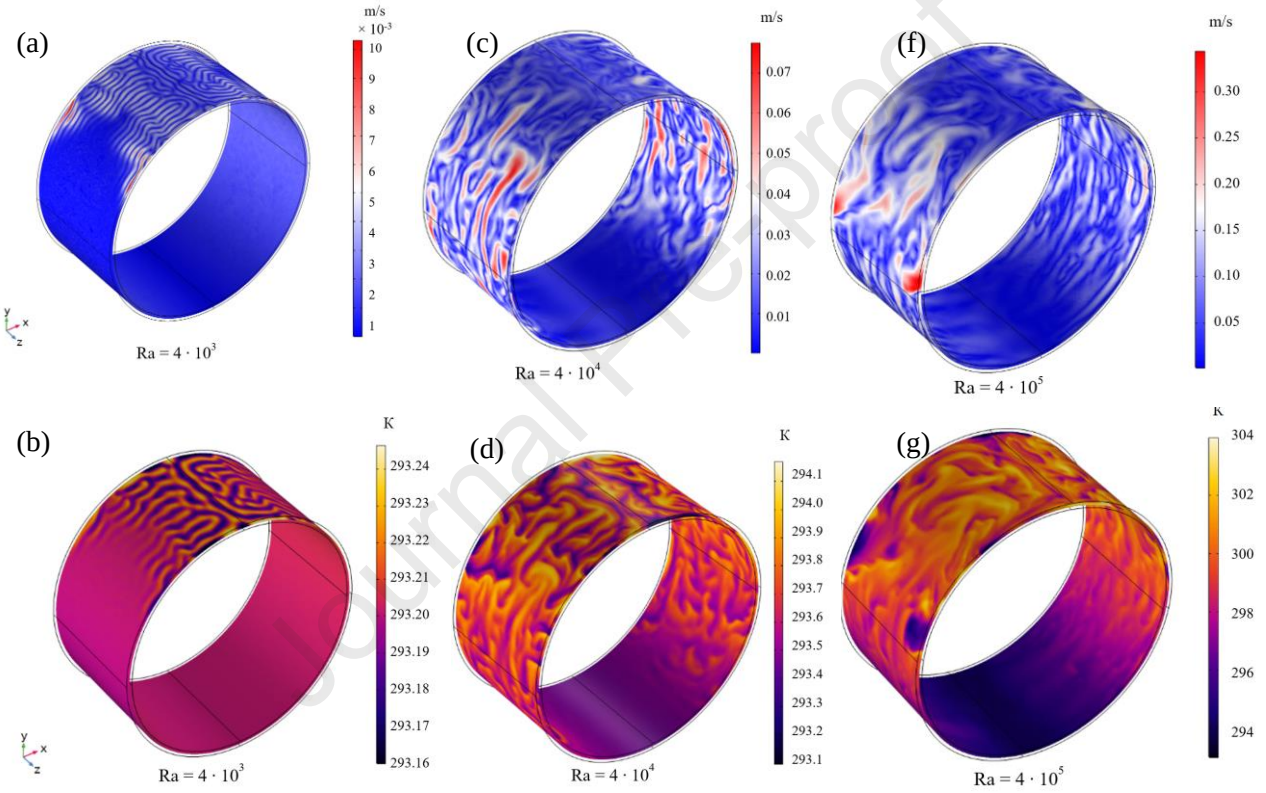

Figure 3. Slices of the velocity and temperature fields for the 3D problem at half-width of a cylindrical layer.
Velocity for different Ra: (a) – $4 \cdot 10^3$, (c) – $4 \cdot 10^4$, (f) – $4 \cdot 10^5$.
Temperature for different Ra: (b) – $4 \cdot 10^3$, (d) – $4 \cdot 10^4$, (g) – $4 \cdot 10^5$.

4. Heat loading and dynamic properties

4.1 Heat loading

The heat loading is a quantity of heat that can be removed from a system during the heat transfer process. The heat loading was estimated as the time-averaged heat flux at the cold boundary q_n. The angular distributions of q_n are given in Figure 4a,b. As we see, q_n is periodic in the upper region for Ra = $4 \cdot 10^3$ due to the spatial periodicity of stable convective rolls (Figure 2a,b and Figure 3a,b).

With the increase of Ra up to $4 \cdot 10^4$, the heat flux remains periodic for the 2D case (Figure 4a). However, for the 3D case, the convection pattern becomes quasistationary (see Figure 3c,d) and q_n loses its periodicity after time-averaging (Figure 4b). With the further increase of Ra, spatial

oscillations in q_n disappear.

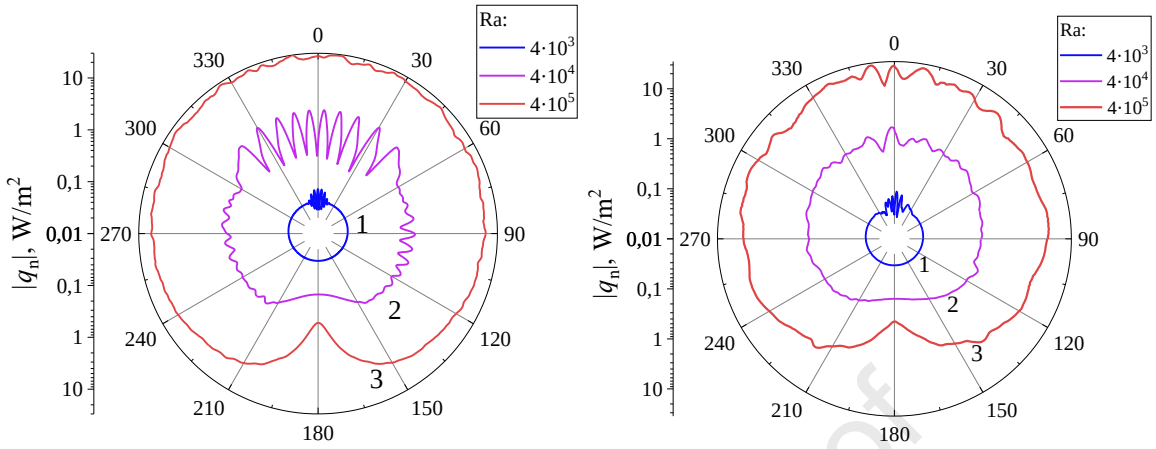

(a) (b)

Figure 4. The angular distribution of the heat flux at the cold boundary q_n for the 2D (a) and 3D (b) problems for different Ra: 1 – $4\cdot10^3$, 2 – $4\cdot10^4$, 3 – $4\cdot10^5$

4.2 Nusselt number

The Nusselt number defines the contribution of convection to overall heat transfer [55]. It was calculated as the ratio of overall heat flux q_n at a cold boundary to flux q_n^{cond} for a system with a heat conduction mechanism only [55]:

$$\mathrm{Nu} = \frac{\int_0^{2\pi} q_n(\varphi)\mathrm{d}\varphi}{\int_0^{2\pi} q_n^{cond}(\varphi)\mathrm{d}\varphi}. \qquad (8)$$

The dependence of Nu on the Rayleigh number is given in Figure 5. As we can see, values of the Nusselt number for thin layers (points on the dotted lines 1 and 2) are a few times lower than Nu for classical RB-convection (solid line 4) [56] and Nu for a thick cylindrical layer (dashed line 3) [57]. Lower values of Nu for thin cylindrical layers may be explained by the existence of a region at the bottom of the layer where convection is not going on because the hot boundary is above the cold one.

For a thin cylindrical layer, the 2D problem shows a higher Nu number than the 3D one. The difference between Nu for 2D and 3D problems is about 5% for Ra = $4\cdot10^4$ and rapidly increases to 47% for Ra = $4\cdot10^5$. We approximated our simulated data with the power law and found that the Nusselt number for the 2D case is proportional to $0{,}0019\cdot\mathrm{Ra}^{0{,}567}$ and for the 3D case is proportional to $0{,}22\cdot\mathrm{Ra}^{0{,}192}$.

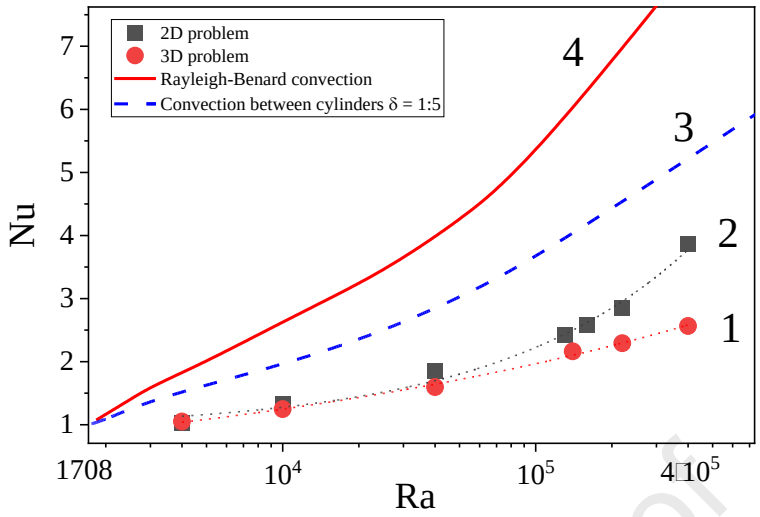

Figure 5. The Nusselt number dependence on the Rayleigh number for different systems:
1 – the 3D problem, 2 – the 2D problem,
3 – the Rayleigh-Bénard convection [56], 4 – the convection between cylinders with δ = 1:5 [57]

4.3 Lyapunov exponent

To better visualize the mixing in the flow, we computed the Lyapunov exponent Λ given in Figure 6. In the 2D case, the Λ is highest at the lateral sides ("butterfly shape", Figure 6a-c). In the 3D case, the highest values of Λ shift down as Ra increases (Figure 6d-g).

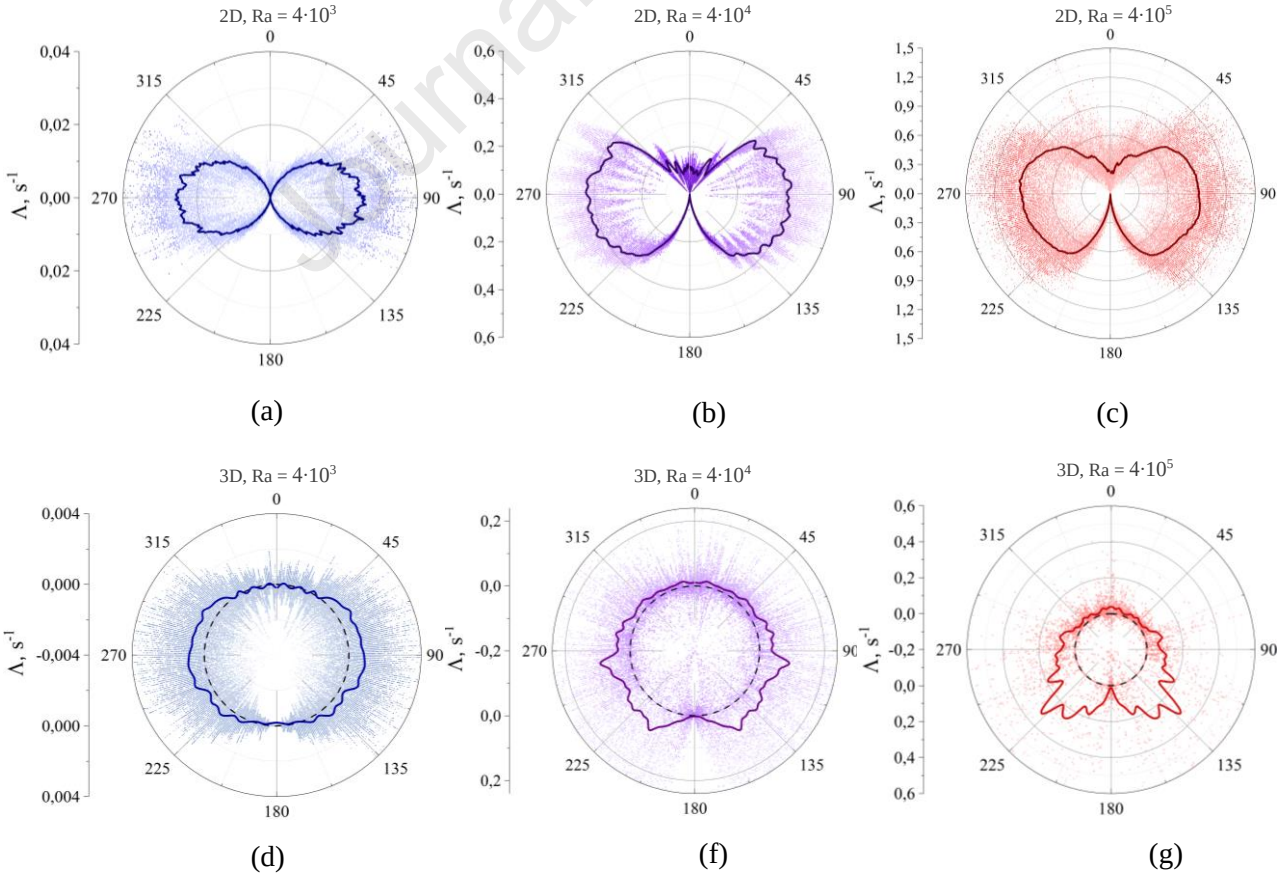

Figure 6. The Lyapunov exponent Λ angular dependence for the 2D (a)-(c) and the 3D (d)-(g) problem at different Rayleigh numbers:
(a), (d) – $4 \cdot 10^3$; (b), (f) – $4 \cdot 10^4$; (c), (g) – $4 \cdot 10^5$.
Solid line is the average value, points are Λ_j for specific pairs of marker particles.

For Ra = $4 \cdot 10^3$, Λ is higher by an order of magnitude for the 2D problem than for the 3D one (Figure 6a,d). This is caused by the 3D convective roll pattern (Figure 3a,b), which makes only half of the fluid involved in convection, while the other fluid remains still and non-intermixing.

It must be noted that the absolute values of Λ are larger for the 2D problem. This qualitatively agrees with a higher Nusselt number because intermixing increase usually intensifies heat transfer [58,59].

5. Conclusions

The numerical study of free convection in a thin cylindrical layer at Rayleigh number in range ($4 \cdot 10^3 \div 4 \cdot 10^5$) was presented in this work. The following conclusions can be made:

1. It was established that convective flow consists of three regions with different dynamics: (i) the upper region with Rayleigh-Bénard cells; (ii) the transitional regions with asymmetric convective cells; and (iii) the lateral regions with transient flow without stable cells;
2. For the 3D problems, the roll convective pattern was observed at the Rayleigh number of $4 \cdot 10^3$, which changed to the plume pattern at the Rayleigh number $4 \cdot 10^4$;
3. The analysis of the Lyapunov exponent revealed that fluid mixing in the 2D problem is more intense than in the 3D one. This is consistent with the more intense heat transfer found for the 2D problem;
4. It was found that for low Rayleigh numbers, the 2D problem may be used to provide a reasonable estimate of the heat transfer rate. The Nusselt number obtained from the 2D problem overestimated Nu from 3D problem by 5% at Rayleigh number $4 \cdot 10^4$ and by 47% at Rayleigh number $4 \cdot 10^5$;
5. It was shown that Nusselt number depends on Rayleigh as $0{,}0019 \cdot \mathrm{Ra}^{0{,}567}$ for the 2D problem and as $0{,}22 \cdot \mathrm{Ra}^{0{,}192}$ for the 3D problem of free convection in the thin cylindrical layer.

Acknowledgements

This research was made possible thanks to a “Nature Inspired Engineering: Nano and Micro dimensional technologies for the economy of the future” project of the Federal Academic Leadership Program “Priority 2030”.

We thank Dr. Olga Fedotova from Scientific-Practical Materials Research Centre of NAS of Belarus (Minsk, Belarus) and Ilya Zur from Institute for Nuclear Problems of Belarusian State University (Minsk, Belarus) for valuable discussions during the preparation of manuscript.

APPENDIX A – CODE VERIFICATION

In order to check if COMSOL Multiphysics is able to accurately solve the free convection problems we reproduced the classical Rayleigh-Bénard convection and compared the results to the literature data.

1. Two-dimensional free convection

The problem was set up for the system of equations (1) on the computational domain given in Figure 7. We considered plane-parallel solid walls with the temperature T_{cold} at the top Γ_u and the temperature T_{hot} at the bottom Γ_b boundary with periodic conditions at the left Γ_{p1} and right Γ_{p2} boundary:

$$\vec{v} = 0,\ y \in \Gamma_b;\ \ \vec{v} = 0,\ y \in \Gamma_u;\ \ \ T = T_{hot},\ y \in \Gamma_b;\ \ T = T_{cold},\ y \in \Gamma_u;\ \ \ \ \vec{v}\big|_{x=0} = \vec{v}\big|_{x=x_{\max}};\ T\big|_{x=0} = T\big|_{x=x_{\max}} \quad (9)$$

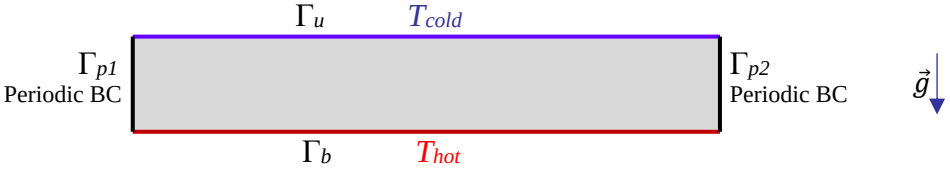

Figure 7. Computational domain for the two-dimensional free convection problem

Equations (1) with conditions (9) were solved using finite-element method implemented in COMSOL Multiphysics [33]. Pressure, velocity and temperature were approximated by a second-order polynomial functions. The mesh included $1 \cdot 10^5$ triangular elements. The velocity magnitude and temperature fields are shown in Fig. 8. Both fields are similar to the reported in literature for Rayleigh-Bénard convection [60–62].

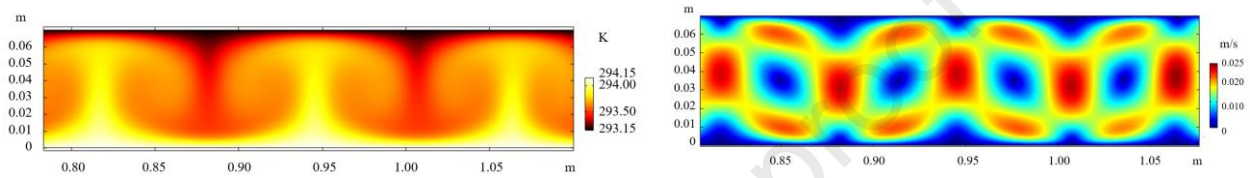

Figure 8. Spatial distributions of (a) temperature and (b) velocity magnitude for the two-dimensional free convection problem at Ra = $2 \cdot 10^4$

We compare vertical profiles of temperature from our work with the profiles given in work [63]. As can be seen from Fig. 9, simulated data is close to the data from [63]. Temperature profile obtained in our simulations is a bit smoother, which may be related to the features of the finite element method used in COMSOL, which solves equations in a weak form with spatial averaging across the mesh cells.

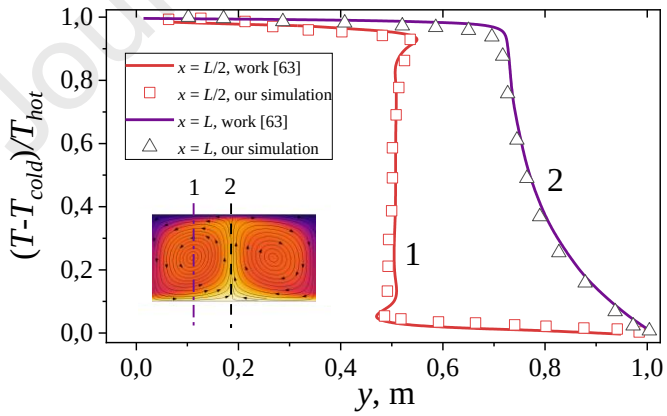

Figure 9. Vertical temperature profiles for 2D convection problem (solid lines – literature data, points – our simulation) at Ra = $2 \cdot 10^4$: 1 – profile between counter-rotating vortices, 2 – profile through the center of vortex. Inset: scheme of convective cell with marked profiles.

2. Three-dimensional free convection

The problem was set up for the system of equations (1) on the computational domain given in Figure 10. We considered plane-parallel solid walls with the temperature T_{cold} at the top Γ_u and the temperature T_{hot} at the bottom Γ_b boundary, periodic conditions at the left Γ_{p1} and right Γ_{p2} boundary and periodic conditions at the front Γ_{p3} and back Γ_{p4} boundary:

$$\vec{v} = 0,\ z \in \Gamma_b;\ \vec{v} = 0,\ z \in \Gamma_u;\ T = T_{hot},\ z \in \Gamma_b;\ T = T_{cold},\ z \in \Gamma_u;$$
$$\vec{v}\big|_{x=0} = \vec{v}\big|_{x=x_{max}};\ T\big|_{x=0} = T\big|_{x=x_{max}};\ \vec{v}\big|_{y=0} = \vec{v}\big|_{y=y_{max}};\ T\big|_{y=0} = T\big|_{y=y_{max}} \quad (10)$$

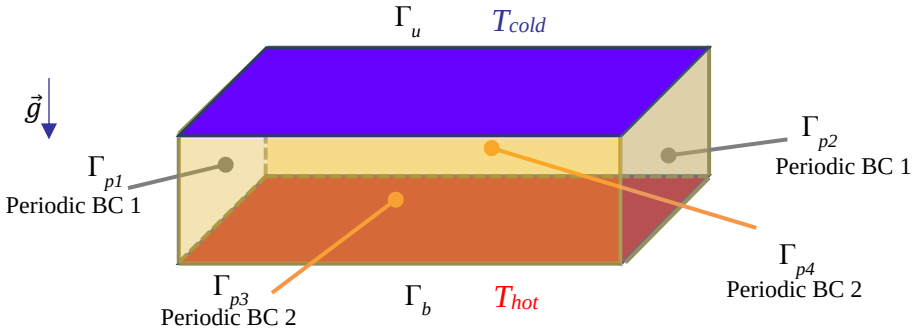

Figure 10. Computational domain for the two-dimensional free convection problem

The computational mesh included $7 \cdot 10^5$ tetrahedral elements. Most of the publications provide information about convective patterns. In Figure 11 there is a comparison between a convective pattern obtained from our simulations in COMSOL and literature data.

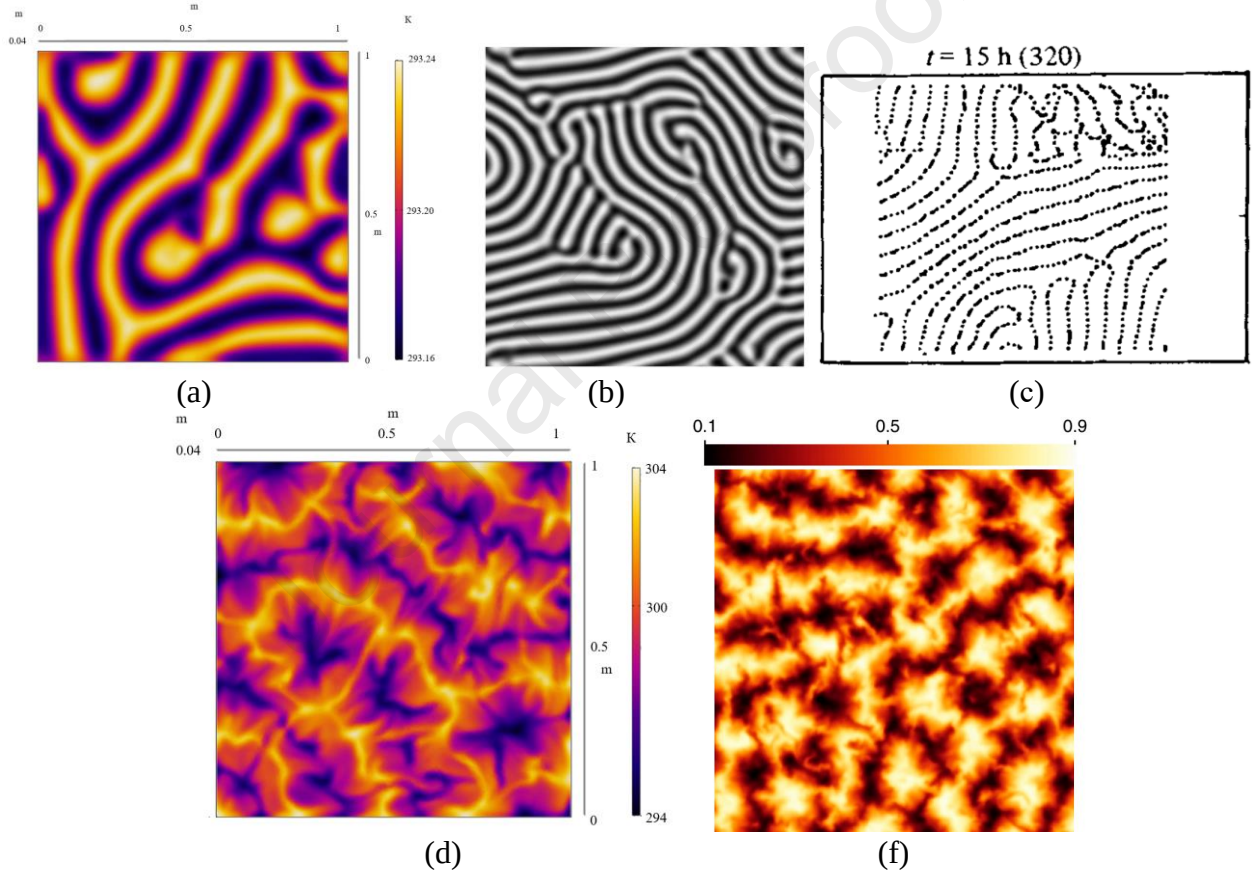

Figure 11. Temperature distribution in the midplane between the upper Γ_u and bottom Γ_b boundaries for the three-dimensional free convection:
(a) – temperature field from our simulations at Ra ≈ $4 \cdot 10^3$;
(b) – convection pattern from simulations [64] at Ra ≈ $3{,}4 \cdot 10^3$;
(c) – isothermal contours from experiment [65] at Ra ≈ $4 \cdot 10^3$;
(d) – temperature field from our simulations at Ra ≈ 10^5;
(f) – temperature field from simulations [64] at Ra ≈ 10^5.

It can be seen, that convective patterns simulated using the COMSOL are close to the literature data available. Small divergence between Fig.11d and Fig.11f can be attributed to a difference in color maps and lower Pr number in work [66]. Summarizing the above, it seems that COMSOL Multiphysics is able to reproduce significant features of free convective flow and can be used for this type of computational studies.

Bibliography

[1] R. A. Houze, *Cloud Dynamics*, 2nd ed. (Elsevier Science, 2014).

[2] D. Weairet and N. Rivier, *Soap, Cells and Statistics-Random Patterns in Two Dimensions*, Contemp. Phys. **25**, 59 (1984).

[3] R. J. Ray, W. B. Krantz, T. N. Caine, and R. D. Gunn, *A Model for Sorted Patterned-Ground Regularity.*, J. Glaciol. **29**, 317 (1983).

[4] Å. Nordlund, R. F. Stein, and M. Asplund, *Solar Surface Convection*, Living Rev. Sol. Phys. **6**, (2009).

[5] W. J. Stępniowski, M. Norek, M. Michalska-Domańska, D. Forbot, and A. Król, *Study on the Correlation between Criterion Number Derived from Rayleigh-Bénard Convective Cells and Arrangement of Nanoporous Anodic Aluminum Oxide*, Mater. Lett. **125**, 124 (2014).

[6] J. Ahuja and J. Sharma, *Rayleigh–Bénard Instability in Nanofluids: A Comprehensive Review*, Micro Nano Syst. Lett. **8**, (2020).

[7] W. K. S. Chiu, C. J. Richards, and Y. Jaluria, *Flow Structure and Heat Transfer in a Horizontal Converging Channel Heated from Below*, Phys. Fluids **12**, 2128 (2000).

[8] A. Benderradji, A. Haddad, R. Taher, M. Médale, C. Abid, and F. Papini, *Characterization of Fluid Flow Patterns and Heat Transfer in Horizontal Channel Mixed Convection*, Heat Mass Transf. Und Stoffuebertragung **44**, 1465 (2008).

[9] T. F. Lin, *Buoyancy Driven Vortex Flow and Thermal Structures in a Very Low Reynolds Number Mixed Convective Gas Flow through a Horizontal Channel*, Int. J. Heat Fluid Flow **24**, 299 (2003).

[10] A. Averyanov, A. Bazhazhin, V. F. Chepurnov, V. V. Chepurnov, G. Cheremukhina, S. Chernenko, O. Fateev, Y. Kiriushin, A. Kolesnikov, A. Korotkova, F. Levchanovsky, J. Lukstins, S. Movchan, A. Pilyar, S. Razin, A. Ribakov, V. Samsonov, S. Vereschagin, Y. Zanevsky, S. Zaporozhets, and V. Zruev, *TPC Status for MPD Experiment of NICA Project*, J. Instrum. **12**, (2017).

[11] O. G. Romanov, G. G. Krylov, A. S. Fedotov, and Y. D. Tsitavets, Computational Analysis of Heat Transfer in MPD Setup and TPC Thermostabilization System, 2020.

[12] A. S. Fedotov, O. G. Romanov, I. F. Gunter, Y. D. Tsitavets, I. A. Zur, and K. S. Stepanishin, Evaluation of Heat Load to the Working Gas of TPC Detector from Subdetectors of MPD Setup and Measuring TPC Electronics, 2021.

[13] A. Benallou, *Energy Transfers by Convection* (Wiley, London, 2019).

[14] *The TPC Cooling and Temperature Stabilization System*, https://alice-tpc.web.cern.ch/content/tpc-cooling-and-temperature-stabilization-system.

[15] J. Alme, Y. Andres, H. Appelshuser, S. Bablok, N. Bialas, R. Bolgen, U. Bonnes, R. Bramm, P. Braun-Munzinger, R. Campagnolo, P. Christiansen, A. Dobrin, C. Engster, D. Fehlker, Y. Foka, U. Frankenfeld, J. J. Gaardhøje, C. Garabatos, P. Glssel, C. Gonzalez Gutierrez, P. Gros, H. A. Gustafsson, H. Helstrup, M. Hoch, M. Ivanov, R. Janik, A. Junique, A. Kalweit, R. Keidel, S. Kniege, M. Kowalski, D. T. Larsen, Y. Lesenechal, P. Lenoir, N. Lindegaard, C. Lippmann, M. Mager, M. Mast, A. Matyja, M. Munkejord, L. Musa, B. S. Nielsen, V. Nikolic, H. Oeschler, E. K. Olsen, A. Oskarsson, L. Osterman, M. Pikna, A. Rehman, G. Renault, R. Renfordt, S. Rossegger, D. Rhrich, K. Røed, M. Richter, G. Rueshmann, A. Rybicki, H. Sann, H. R. Schmidt, M. Siska, B. Sitr, C. Soegaard, H. K. Soltveit, D. Soyk, J. Stachel, H. Stelzer, E. Stenlund, R. Stock, P. Strme, I. Szarka, K. Ullaland, D. Vranic, R. Veenhof, J. Westergaard, J. Wiechula, and B. Windelband, *The ALICE TPC, a Large 3-Dimensional Tracking Device with Fast Readout for Ultra-High Multiplicity Events*, Nucl. Instruments Methods Phys. Res. Sect. A Accel. Spectrometers, Detect. Assoc. Equip. **622**, 316 (2010).

[16] J. Yoo, *Natural Convection in a Narrow Horizontal Cylindrical Annulus: Pr ≤ 0.3*, Int. J. Heat Mass Transf. **41**, 3055 (1998).

[17] A. Passerini, C. Ferrario, M. Ružička, and G. Thäter, *Theoretical Results on Steady Convective Flows between Horizontal Coaxial Cylinders**, SIAM J. Appl. Math. **71**, 465 (2011).

[18] Y. Wang, J. Chen, and W. Zhang, *Natural Convection in a Circular Enclosure with an Internal Cylinder of Regular Polygon Geometry*, AIP Adv. **9**, (2019).

[19] H. S. Majdi, L. J. Habeeb, M. Elmnifi, and N. Alderoubi, *Transient Free Convection between Two Horizontal Concentric Cylinders*, Int. J. Mech. Eng. **7**, 596 (2022).

[20] J. Yoo, *Flow Pattern Transition of Natural Convection in a Horizontal Annulus with Constant Heat Flux on the Inner Wall*, Int. J. Numer. Methods Heat Fluid Flow **15**, 698 (2005).

[21] H. Laidoudi, A. K. Hussein, A. B. Mahdi, O. Younis, E. H. Malekshah, H. Togun, and U. Biswal, *Numerical Investigation of Buoyancy-Driven Flow in a Crescentshaped Enclosure*, Jordan J. Mech. Ind. Eng. **16**, 627 (2022).

[22] F. H. Ali, H. K. Hamzah, A. K. Hussein, M. Y. Jabbar, and P. Talebizadehsardari, *MHD Mixed Convection Due to a Rotating Circular Cylinder in a Trapezoidal Enclosure Filled with a Nanofluid Saturated with a Porous Media*, Int. J. Mech. Sci. **181**, 105688 (2020).

[23] S. H. Hussain and A. K. Hussein, *Mixed Convection Heat Transfer in a Differentially Heated Square Enclosure with a Conductive Rotating Circular Cylinder at Different Vertical Locations*, Int. Commun. Heat Mass Transf. **38**, 263 (2011).

[24] A. K. Hussein, H. K. Hamzah, F. H. Ali, and L. Kolsi, *Mixed Convection in a Trapezoidal Enclosure Filled with Two Layers of Nanofluid and Porous Media with a Rotating Circular Cylinder and a Sinusoidal Bottom*

Wall, J. Therm. Anal. Calorim. **141**, 2061 (2020).
[25] Z. K. Ghoben and A. K. Hussein, *The Natural Convection inside a 3D Triangular Cross Section Cavity Filled with Nanofluid and Included Cylinder with Different Arrangements*, Diagnostyka **23**, 1 (2022).
[26] S. Gourari, F. Mebarek-Oudina, A. K. Hussein, L. Kolsi, W. Hassen, and O. Younis, *Numerical Study of Natural Convection between Two Coaxial Inclined Cylinders*, Int. J. Heat Technol. **37**, 779 (2019).
[27] B. Mallikarjuna, A. M. Rashad, A. K. Hussein, and S. Hariprasad Raju, *Transpiration and Thermophoresis Effects on Non-Darcy Convective Flow Past a Rotating Cone with Thermal Radiation*, Arab. J. Sci. Eng. **41**, 4691 (2016).
[28] M. I. Elkhazen, W. Hassen, R. Gannoun, A. K. Hussein, and M. N. Borjini, *Numerical Study of Electroconvection in a Dielectric Layer Between Two Cofocal Elliptical Cylinders Subjected to Unipolar Injection*, J. Eng. Phys. Thermophys. **92**, 1318 (2019).
[29] I. D. Erhunmwun and U. B. Ikponmwosa, *Review on Finite Element Method*, J. Appl. Sci. Environ. Manag. **21**, 999 (2017).
[30] E. Dick, *Introduction to Finite Element Methods in Computational Fluid Dynamics*, in *Computational Fluid Dynamics* (2009), pp. 235–274.
[31] S. V. Patankar, *Numerical Heat Transfer and Fluid Flow.*, 214 (1980).
[32] F. Bassani, D. Poggi, L. Ridolfi, and J. Von Hardenberg, *Rayleigh-Bénard Convection with Thermal Boundary Inhomogeneities*, Phys. Rev. E **105**, 1 (2022).
[33] COMSOL AB, *COMSOL Multiphysics*, www.comsol.com.
[34] P. B. Gibbons, *ACM Transactions on Parallel Computing: An Introduction*, ACM Trans. Parallel Comput. **1**, (2014).
[35] M. Bollhöfer, O. Schenk, R. Janalik, S. Hamm, and K. Gullapalli, *State-of-the-Art Sparse Direct Solvers*, Model. Simul. Sci. Eng. Technol. 3 (2020).
[36] M. Bollhöfer, A. Eftekhari, S. Scheidegger, and O. Schenk, *Large-Scale Sparse Inverse Covariance Matrix Estimation*, SIAM J. Sci. Comput. **41**, A380 (2019).
[37] P. N. Brown, A. C. Hindmarsh, and L. R. Petzold, *Using Krylov Methods in the Solution of Large-Scale Differential-Algebraic Systems*, SIAM J. Sci. Comput. **15**, 1467 (1994).
[38] A. C. Hindmarsh, P. N. Brown, K. E. Grant, S. L. Lee, R. Serban, D. E. Shumaker, and C. S. Woodward, *SUNDIALS: Suite of Nonlinear and Differential/Algebraic Equation Solvers*, ACM Trans. Math. Softw. **31**, 363 (2005).
[39] P. K. Moore and L. R. Petzold, *A Stepsize Control Strategy for Stiff Systems of Ordinary Differential Equations*, Appl. Numer. Math. **15**, 449 (1994).
[40] B. F. Wang, Q. Zhou, and C. Sun, *Vibration-Induced Boundary-Layer Destabilization Achieves Massive Heat-Transport Enhancement*, Sci. Adv. **6**, (2020).
[41] Y. Zhang, Q. Zhou, and C. Sun, *Statistics of Kinetic and Thermal Energy Dissipation Rates in Two-Dimensional Turbulent Rayleigh-Bénard Convection*, J. Fluid Mech. **814**, 165 (2017).
[42] J. L. Yang, Y. Z. Zhang, T. C. Jin, Y. H. Dong, B. F. Wang, and Q. Zhou, *The-Dependence of the Critical Roughness Height in Two-Dimensional Turbulent Rayleigh-Bénard Convection*, J. Fluid Mech. **911**, (2021).
[43] J. C. Vallejo and M. A. F. Sanjuan, *Predictability of Chaotic Dynamics* (2017).
[44] R. C. Hilborn, *Lyapunov Exponents: A Tool to Explore Complex Dynamics*, Vol. 70 (2017).
[45] *Particle Tracing Module Application Library Manual* (Comsol, 2017).
[46] P. J. Prince and J. R. Dormand, *High Order Embedded Runge-Kutta Formulae*, J. Comput. Appl. Math. **7**, 67 (1981).
[47] A. Wolf, J. B. Swift, H. L. Swinney, and J. A. Vastano, *Determining Lyapunov Exponents from a Time Series*, Phys. D Nonlinear Phenom. **16**, 285 (1985).
[48] E. E. Fedoseev, V. V. Kolmychkov, and O. S. Mazhorova, *3D Computer Simulation of Rayleigh-Benard Instability in a Square Box*, Prog. Comput. Fluid Dyn. **10**, 208 (2010).
[49] H. Kurtuldu, K. Mischaikow, and M. F. Schatz, *Measuring the Departures from the Boussinesq Approximation in Rayleigh-BÃnard Convection Experiments*, J. Fluid Mech. **682**, 543 (2011).
[50] F. Zhong and R. Ecke, *Pattern Dynamics and Heat Transport in Rotating Rayleigh-Bénard Convection*, Chaos **2**, 163 (1992).
[51] P. Manneville, *Rayleigh-Bénard Convection: Thirty Years of Experimental, Theoretical, and Modeling Work*, 41 (2006).
[52] A. Turing, *The Chemical Basis of Morphogenesis*, Philos. Trans. R. Soc. Lond. B. Biol. Sci. **237**, 37 (1952).
[53] A. Banerjee, *Rayleigh-Taylor Instability: A Status Review of Experimental Designs and Measurement Diagnostics*, J. Fluids Eng. **142**, (2020).
[54] H. J. Kull, *Theory of the Rayleigh-Taylor Instability*, Phys. Rep. **206**, 197 (1991).
[55] F. M. White, *Heat Transfer* (Addison-Wesley, 1984).
[56] X. He, S. Chen, and G. D. Doolen, *A Novel Thermal Model for the Lattice Boltzmann Method in Incompressible Limit*, J. Comput. Phys. **146**, 282 (1998).
[57] T. H. Kuehn and R. J. Goldstein, *An Experimental and Theoretical Study of Natural Convection in the Annulus between Horizontal Concentric Cylinders*, J. Fluid Mech. **74**, 695 (1976).
[58] A. Sinha, H. Chattopadhyay, A. K. Iyengar, and G. Biswas, *Enhancement of Heat Transfer in a Fin-Tube Heat Exchanger Using Rectangular Winglet Type Vortex Generators*, Int. J. Heat Mass Transf. **101**, 667 (2016).
[59] E. K. Kalinin and G. A. Dreitser, *Heat Transfer Enhancement in Heat Exchangers*, Adv. Heat Transf. **31**, 159

(1998).
[60] A. R. Rahmati, M. Ashrafizadeh, and E. Shirani, *Novel Hybrid Finite-Difference Thermal Lattice Boltzmann Models for Convective Flows*, Heat Transf. Res. **40**, 747 (2009).
[61] C. D. Andereck, P. W. Colovas, M. M. Degen, and Y. Y. Renardy, *Instabilities in Two Layer Rayleigh–Bénard Convection: Overview and Outlook*, Int. J. Eng. Sci. **36**, 1451 (1998).
[62] Lord Rayleigh, *LIX. On Convection Currents in a Horizontal Layer of Fluid, When the Higher Temperature Is on the under Side*, London, Edinburgh, Dublin Philos. Mag. J. Sci. **32**, 529 (1916).
[63] D. R. Moore and N. O. Weiss, *Two-Dimensional Rayleigh-Benard Convection*, J. Fluid Mech. **58**, 289 (1973).
[64] J. D. Scheel, Rotating Rayleigh-Benard Convection, California Institute of Technology, 2007.
[65] J. P. Gollub, A. R. Mccarriar, and J. F. Steinman, *Convective Pattern Evolution and Secondary Instabilities*, J. Fluid Mech. **125**, 259 (1982).
[66] A. Pandey, J. D. Scheel, and J. Schumacher, *Turbulent Superstructures in Rayleigh-Bénard Convection*, Nat. Commun. **9**, (2018).

Alexander Fedotov: Methodology, Writing - Review & Editing, Software **Yana Tsitavets**: Software, Investigation, Original draft preparation. **Andrey Elyshev**: Visualization, Investigation, Conceptualization, Writing - Review & Editing

Declaration of interests

☒ The authors declare that they have no known competing financial interests or personal relationships that could have appeared to influence the work reported in this paper.

☐ The authors declare the following financial interests/personal relationships which may be considered as potential competing interests: